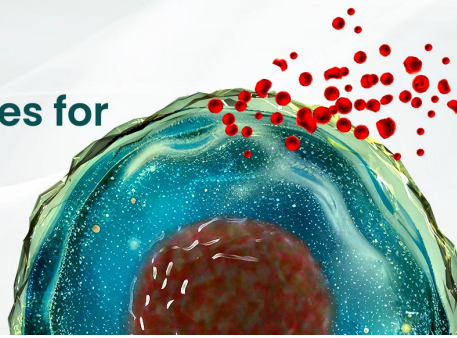




BEST-IN-CLASS Cytokines for BEST Cell Culture

Sino Biological Named 'Growth Factor
Supplier to Watch in 2024' by CiteAb



Learn
More

The Journal of Immunology

RESEARCH ARTICLE | MARCH 22 2023

TLR5-Derived, TIR-Interacting Decoy Peptides to Inhibit TLR Signaling

Artur Javmen; ... et. al

J Immunol (2023) 210 (9): 1419–1427.

<https://doi.org/10.4049/jimmunol.2200394>

Related Content

Diversity of gut commensal flagellins results in distinct intestinal epithelial cell immune responses

J Immunol (May,2023)

Targeting the TLR7 signalosome assembly by TLR7-derived decoy peptides

J Immunol (May,2020)

TLR5-Derived, TIR-Interacting Decoy Peptides to Inhibit TLR Signaling

Artur Javmen,* Jun Zou,[†] Shreeram C. Nallar,* Henryk Szmanski,[‡] Joseph R. Lakowicz,[‡] Andrew T. Gewirtz,[†] and Vladimir Y. Toshchakov*

TLR5, which is activated by flagellin, plays an important role in initiating immune response to a broad spectrum of motile bacterial pathogens. TLRs induce intracellular signaling via dimerization of their TIR domains followed by adapter recruitment through multiple interactions of receptor and adapter TIRs. Here, a library of cell-permeable decoy peptides derived from the TLR5 TIR was screened for TLR5 signaling inhibition in the HEK-Blue-mTLR5 reporter cell line. The peptide demonstrating the strongest inhibition, 5R667, corresponded to the second helix of the region between the third and fourth β -strands (helix C''). In addition to the TLR5-induced cytokine expression, 5R667 inhibited cytokine expression elicited by TLR4, TLR2, and TLR9. 5R667 also suppressed the systemic cytokine induction elicited by LPS administration in mice. 5R667 binding specificity was studied by time-resolved fluorescence spectroscopy in a cell-based assay. 5R667 demonstrated a multispecific binding pattern with respect to TIR domains: It bound TIRs of TLR adapters of the MyD88-dependent pathway, Toll/interleukin-1 receptor domain-containing adapter protein/MyD88 adapter-like (TIRAP) and MyD88, and also the TIR of TLR5. TR667, the peptide derived from the TIRAP region, which is structurally homologous to 5R667, demonstrated binding and inhibitory properties similar to that of 5R667. The surface-exposed residues within TIR regions represented by 5R667 and TR667 form motifs, which are nearly 90% conserved in vertebrate evolution and are distinctive of TLR5 and TIRAP TIR domains. Thus, we have identified an evolutionary conserved adapter recruitment motif within TLR5 TIR, the function of which can be inhibited by selective cell-permeable decoy peptides, which can serve as pan-specific TLR inhibitors. *The Journal of Immunology*, 2023, 210: 1419–1427.

Toll-like receptors recognize microbial pattern molecules and initiate host immune response critical for infection resolution (1, 2). TLR5 is activated by bacterial protein flagellin and thus is important for detection of a wide range of motile bacterial pathogens (3, 4). Flagellin also activates nucleotide-binding, leucine-rich repeat, and caspase activation and recruitment domain containing protein 4 (NLRC4) inflammasome, a cytoplasmic signaling complex that activates proinflammatory and proapoptotic caspases (5–7). The TLR5 signaling depends on adapter protein MyD88 (4); it was also reported that the TLR5 signaling is enhanced in the presence of TIR domain-containing adapter-inducing IFN- β adapter protein in intestinal epithelial cells (8). Activated TLRs dimerize their Toll/IL-1R resistance (TIR) domains and thereby initiate the formation of intracellular signaling complexes through multiple, cooperative interactions of TLR TIR domains with TIR domains of TLR adapters (9–11). Recent studies have suggested the modes of TIR domain interactions that underlie the formation of functional signaling complexes (12–14).

Peptides derived from protein interaction sites can often suppress interactions mediated by corresponding sites and, consequently, downstream protein functions. Such peptides (often referred to as “decoy peptides”) are of growing interest in protein studies and development of therapeutic interventions (14–16). Small decoy peptides that represent linear segments of protein–protein interaction sites can be delivered to intracellular targets by addition of a cell-permeating peptide

vector (17, 18). Previous research has characterized many TIR domain-derived cell-permeating peptides that suppress TLR signaling (14, 19). Our new study presents results of screening of TLR5 TIR-derived decoy peptides and characterizes new peptides that suppress TLR signaling.

Materials and Methods

Animals and cells

Cell-permeable peptides were screened for TLR5 inhibition using HEK-Blue-mTLR5 cells stably transfected with mouse TLR5 (InvivoGen, San Diego, CA). Peritoneal macrophages were obtained by peritoneal lavage from C57BL/6J mice i.p. administered 3% thioglycolate broth (Remel, San Diego, CA), 4 d prior to macrophage harvesting. Bone marrow–derived macrophages (BMDMs) were obtained as described previously (13). Eight-week-old female wild-type C57BL/6 mice were purchased from The Jackson Laboratory (Bar Harbor, ME). NLRC4-deficient mice on the C57BL/6J background were kindly provided by Vishva Dixit (Genentech, South San Francisco, CA).

TLR agonists and decoy peptides

The FliC isoform of flagellin was HPLC purified, and purity was verified as previously described (3, 20–22). Phenol-purified *Escherichia coli* K235 LPS40 was a kind gift of Dr. Stefanie N. Vogel (University of Maryland School of Medicine, Baltimore, MD). R848, S-(2,3-bis (palmitoyloxy)-(2R,2S)-propyl)-N-palmitoyl-(R)-Cys-Ser-Lys₄-OH (P3C), and ODN1668 were purchased from InvivoGen (San Diego, CA).

*Department of Microbiology and Immunology, University of Maryland School of Medicine, Baltimore, MD; [†]Institute for Biomedical Sciences, Georgia State University, Atlanta, GA; and [‡]Center for Fluorescence Spectroscopy, Department of Biochemistry and Molecular Biology, University of Maryland School of Medicine, Baltimore, MD

ORCIDs: 0000-0003-1812-7424 (S.C.N.); 0009-0007-7600-2714 (H.S.); 0000-0002-6338-7578 (A.T.G.); 0000-0002-7942-2294 (V.Y.T.).

Received for publication June 2, 2022. Accepted for publication February 22, 2023.

This work was supported in part by the following National Institutes of Health grants: AI082299 (V.Y.T.), GM144147 and GM125976 (J.R.L.), and DK099071 (A.T.G.).

Address correspondence and reprint requests to Dr. Vladimir Y. Toshchakov, University of Maryland School of Medicine, 685 West Baltimore Street, HSF1 Suite 380, Baltimore, MD 21201. E-mail address: vtoshchakov@som.umaryland.edu

The online version of this article contains supplemental material.

Abbreviations used in this article: BMDM, bone marrow–derived macrophage; Cer, Cerulean fluorescent protein; FLIM, Fluorescence lifetime imaging; FRET, Förster resonance energy transfer; KC, keratinocyte chemoattractant; NLRC4, nucleotide-binding leucine-rich repeat and caspase activation and recruitment domain containing protein 4; P3C, S-(2,3-bis (palmitoyloxy)-(2R,2S)-propyl)-N-palmitoyl-(R)-Cys-Ser-Lys₄-OH; TIR, Toll/IL-1R resistance; TIRAP, Toll/interleukin-1 receptor domain-containing adapter protein/MyD88 adapter-like.

Copyright © 2023 by The American Association of Immunologists, Inc. 0022-1767/23/\$37.50

Decoy peptides were synthesized by Aapptec (Louisville, KY) or GenScript (Piscataway, NJ). All peptides were supplemented with Antennapedia homeo-domain sequence RQIKIWFAQNRMRKWK (23) positioned N-terminally. Cy3-labeled peptides were produced by CPC Scientific (Sunnyvale, CA). The Cy3 label was placed at the peptide N-terminus. The purity of all peptides used was $\geq 95\%$. Lyophilized peptides were reconstituted in UltraPure water to a concentration of 2 mM. Concentrations of reconstituted peptides were determined spectrophotometrically (24). Peptide stocks were stored at -80°C or directly added to cell culture medium to a final concentration of 20 or 40 μM for in vitro experiments or diluted with PBS to final concentration of 400 μM (200 nmol in 0.5 ml) for administration to mice.

Screening of TLR5 peptides

HEK-Blue-mTLR5 cells were seeded into 96-well plates. Upon reaching $\sim 80\%$ confluence, the cells were preincubated with 20 or 40 μM TLR5 peptides for 30 min and stimulated with FliC (10 ng/ml) for 5 h. Then, supernatants were collected and incubated with QUANTI-Blue for 25 min, followed by alkaline phosphatase activity measurement at 620 nm using a plate reader.

Quantitative real-time PCR

Mouse BMDMs or peritoneal macrophages were obtained as described before (13, 19). The harvested cells were plated into 12-well plates at a density of 2×10^6 cells per well and incubated overnight in 5% CO_2 atmosphere at 37°C . After treatment with TLR agonists and antagonists per experimental conditions, the cells were lysed and mRNA was isolated using TRIzol reagent (Life Technologies, Carlsbad, CA). cDNA was synthesized from 1 μg of isolated mRNA using the RevertAid RT kit (Thermo Fisher Scientific, Waltham, MA). The obtained cDNA was amplified using gene-specific primers for mouse HPRT, TNF- α , IL-1 β , keratinocyte chemoattractant (KC), IL-6, or IL-12p40 and SYBR Green PCR Mix (Applied Biosystems, Foster City, CA) and quantified as described earlier (25). The statistical significance of differences in mRNA expression was evaluated by one-way ANOVA combined with Dunnett's multiple comparison test.

Cytokine detection

Cytokine secretion was measured in cell supernatants or plasma samples stored at -80°C until measurements. Samples were analyzed by mouse IL-6, IL-1 β , IL-22, and TNF- α ELISA kits from BioLegend (San Diego, CA) per the manufacturer's protocols.

Cell viability measurements

Freshly isolated mouse peritoneal macrophages were plated into 96-well plates and incubated overnight in the RPMI medium supplemented with 2% FBS. Cells were treated with decoy peptides at 20 or 40 μM for 22, 4, and 2 h and then incubated for 3 h in the presence of MTT (1.67 mM). Media were aspirated, and cells were lysed in 50 μl of isopropanol supplemented with 0.1% Nonidet P-40 and HCl to 4 mM. The 595-nm absorbance was read after 15-min incubation on a shaker. Control treatments were Triton X-100 (0.1%) and mouse TNF- α (BioLegend, San Diego, CA) together with actinomycin D at 10 ng/ml and 1 $\mu\text{g}/\text{ml}$, respectively. All treatments were set in duplicates.

SDS-PAGE and Western analysis

SDS-PAGE and Western blot analysis were performed as described previously (26) with minor modifications. Rabbit Abs for detection of activated and total ERK isoforms and IKK (I κ B kinase)- α/β phosphorylated on Ser176/180 were purchased from Cell Signaling Technology (Danvers, MA).

Fluorescence lifetime imaging (FLIM)

Cell transfection, slide preparation, and image acquisition and analysis were conducted as described earlier (10, 19, 27). Mammalian expression vectors that encode TIR domains fused with Cerulean fluorescent protein (MyD88-Cer and Toll/interleukin-1 receptor domain-containing adapter protein/MyD88 adapter-like [TIRAP]-Cer) and Cer not fused to a TIR were described previously (28, 29). The TLR5 TIR coding sequence was PCR amplified from a mouse macrophage cDNA library using modifying primers to introduce NheI and Bsu361 cloning sites. The obtained PCR product was recombined into TLR4-Cer pcDNA3.1 Zeo⁽⁻⁾ vector (10) to replace the TLR4 coding sequence, using NheI and Bsu361 sites. All expression vectors were verified by sequencing.

Animal experiments

Systemic cytokine activation in wild-type or NLRC4-deficient C57BL/6 mice was induced by i.p. administration of LPS (10 μg) or flagellin (20 μg). Peptides were administered i.p. at a dose of 200 nmol per mouse as a 0.5-ml PBS aliquot 1 h prior to administration of a TLR agonist. The plasma samples were collected 1, 3, and 5 h after TLR stimulation. Data were collected in

at least three independent experiments. ELISA kits from BioLegend were used to measure systemic cytokine levels.

Structural modeling

The three-dimensional structure of human TLR5 TIR was modeled using RoseTTAFold software through Robetta server (30). The model of TIRAP TIR was obtained from the Protein Data Bank (31), Protein Data Bank file 5uzb (12). Structures were analyzed and visualized using the Swiss-Pdb Viewer (32).

Results

Screening of TLR5 peptide library

The TLR5 peptide library tested comprised 12 peptides. The library was designed such that peptides 5R2–5R11 corresponded to structural elements, each of which forms a nonfragmented patch of TIR surface, whereas peptides 5R1 and 5R12 corresponded to presumably unstructured segments immediately preceding and following the TIR (Fig. 1A). Peptide sequences are presented in Table I. Each peptide included the Antennapedia homeodomain cell-permeating vector (Antp), positioned N-terminally to a TLR5 segment. The initial peptide screening was conducted using HEK-Blue-mTLR5 cells, a human cell line stably transfected with mouse TLR5 and a reporter gene under NF- κ B and AP-1 control. Results of the screening are shown in Fig. 1. Peptides 5R6, 5R7, and 5R11 inhibited the flagellin-induced reporter activation (Fig. 1B). Two of the active peptides, 5R6 and 5R7, represent consecutive segments of the TLR5 primary sequence that correspond to juxtaposed TIR surfaces; therefore, we synthesized and tested two additional peptides, 5R667 and 5R67, each of which partially overlapped with both active peptides. Peptide 5R667 was notably more potent than 5R6 peptide (Fig. 1C); 5R67 demonstrated intermediate results between the two (Fig. 2).

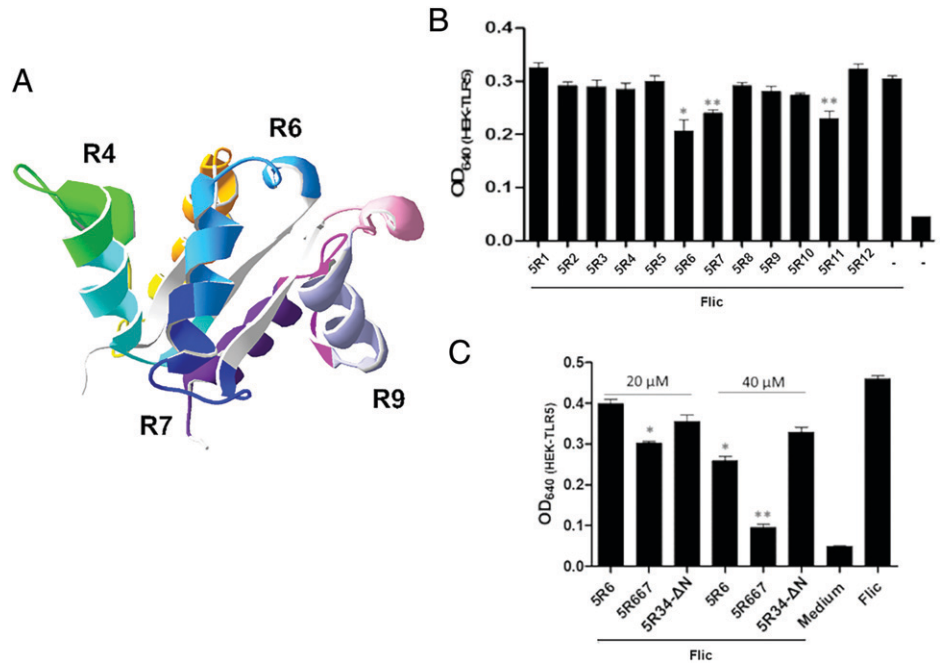
Specificity of TLR inhibition by TLR5-derived peptides

To test the specificity of TLR inhibition by TLR5 peptides and verify inhibitory effects in additional cell lines, 5R6 and its derivatives, 5R67 and 5R667, were tested in primary peritoneal macrophages (pMac) and BMDMs. The TLR5-derived peptides were tested along with a previously identified multispecific TLR inhibitor, peptide 2R9 (29) (a positive control for TLR inhibition), and an inert peptide, 5R12. In addition to positive and negative control peptides, the series was complemented by TIRAP peptides derived from the regions that are structurally homologous to the inhibitory active TLR5 peptides. The sequences of TIRAP peptides, TR6, TR67, and TR667, are presented in Table I. TR6 was described previously as an inhibitor of TLR4 and TLR2 signaling (25), whereas TR667 corresponded to the region that is structurally homologous to that represented by 5R667. Notably, TR667 corresponded to one of two evolutionary conserved TIRAP motifs, which are responsible for receptor–adapter and adapter–adapter interactions for TIRAP (33).

Peritoneal macrophages responded to the FliC stimulation significantly weaker than to LPS, R848, or P3C (Fig. 2A–2D). (Note that the TLR5-stimulated cytokine expression is scaled by a separate y-axis [Fig. 2].) All modifications of 5R6 and TR6 peptides tested suppressed the FliC-induced activation of TNF- α statistically significantly (Fig. 2A), whereas the FliC-induced IL-1 β , IL-12p40, and KC expression was not inhibited significantly. (Note, however, that the IL-12p40 expression was not induced significantly by FliC at the 1 h early time point [Fig. 2B–2D].) 5R6, TR6, and their modifications potentially inhibited the cytokine expression when cells were stimulated with LPS (Fig. 2A–2D).

The R848-elicited expression of TNF- α , IL-1 β , and KC was not affected significantly by the assessed TLR5- and TIRAP-derived peptides (Fig. 2A, 2B, 2D). In contrast, the R848-induced expression of IL-12p40 was inhibited by every inhibitory peptide tested (Fig. 2C); it should be noted, however, that the TLR-dependent

FIGURE 1. Effects of TLR5-derived peptides on TLR5 signaling. HEK-Blue-mTLR5 cells grown to ~80% confluence were pretreated with decoy peptides for 30 min and stimulated with flagellin (FliC). Data are presented as mean ± SE of at least three replicates. **(A)** Segments of TLR5 TIR backbone that correspond to decoy peptides are shown in different colors. **(B)** Decoy peptides were used at 40 μM, FliC at 3.125 ng/ml. Supernatants for reporter gene expression quantification were collected 16 h after FliC stimulation. **(C)** Decoy peptides were used at 20 and 40 μM, FliC at 10 ng/ml. Supernatants for reporter quantification were collected 5 h after cell stimulation. Data are presented as mean ± SE. **p* < 0.05; ***p* < 0.01.



induction of IL-12p40 is delayed compared with induction of TNF-α, IL-1β, or KC (13, 19, 29, 34), suggesting involvement of generally different, gene-specific regulatory mechanisms.

Effects of peptides on the P3C-induced cytokine expression were similar to that on the FliC-induced expression—TNF-α expression was suppressed significantly (Fig. 2A), whereas peptide effects on the expression of other genes were less and not statistically significant (Fig. 2B–2D). Such a pattern may be attributed to a relatively poor expression of the less affected genes by FliC- or P3C-stimulated macrophages (Fig. 2B–2D). Similarly to the FliC-induced KC expression, the TLR4- or TLR2-induced KC expression was less affected than other cytokines measured (Fig. 2D).

BMDMs, unlike primary peritoneal macrophages, strongly respond to TLR9 stimulation (13). We used BMDMs to test if the TLR5 peptides inhibit TLR9 signaling. 5R6, 5R67, and 5R667 potently inhibited the TLR9-dependent cytokine activation, with 5R667 apparently being the most potent of the three (Fig. 2E). FliC activated the cytokine

expression in BMDMs significantly more weakly than ODN1668. Peptides did not cause statistically significant changes in the FliC-treated BMDMs (not shown).

IL-6 transcription is regulated by multiple transcription factors, the synergistic action of which is required for maximal expression (35). Such a complex regulatory mechanism typically manifests in the delayed activation of IL-6 expression compared with the genes predominantly regulated by NF-κB (Figs. 3A, 4C, and Reference 28, for example). To evaluate effects of decoy peptides on the delayed cytokine expression, we measured the LPS-stimulated IL-6 expression in peritoneal macrophages over a 5-h time course. All tested peptides (i.e., 5R667, TR667, and 4BB) significantly decreased IL-6 expression over the entire observation period. Notably, in most conditions, the IL-6 expression in decoy peptide-treated cells was less than 1% of that in LPS-treated macrophages in the absence of an inhibitory peptide (Fig. 3A and 3B). Peptides 5R667 and TR667 also completely blocked the LPS-induced phosphorylation of ERK and

Table I. Sequences of TIR-derived decoy peptides

Peptide	Sequence	Corresponding TIR region
5R1	DHPQGTEPDYKYD	N-terminal segment
5R2	SKDFTWVQNALLKH	AA loop, α-helix A ^a
5R3	DTQYSDQNRFNLC	α-Helix A, AB loop
5R34-ΔN	RFNLCFEERD	AB loop, β-strand B, BB loop
5R4	FEERDFVPGENRIA	β-Strand B, BB loop, α-helix B
4BB	LHYRDFIPGVAIAA	β-Strand B, BB loop, α-helix B
5R5	NIQDAIWNRSRKI	α-Helix B, BC loop
5R6	RHFLRDGWCLEAFS	α-Helices C
TR6	PGFLRDPWCKYQML	α-Helices C
5R67	CLEAFSYAQGRSLS	α-Helix C ^a
5R667	WCLEAFSYAQGR	α-Helix C ^a
TR667	WCKYQMLQALTE	α-Helix C ^a , CD loop
5R7	YAQGRCLSDLNSA	α-Helix C, CD loop, β-strand D
5R8	GSLSQYQLMKH	DD loop, α-helix D
5R89	LMKHQSIRGFVQK	DD loop, α-helix D, DE loop
5R9	HQSIRGFVQKQQ	α-Helix D, DE loop
5R10	QQYLRWPEDLQDV	DE loop, β-strand E, EE loop
5R1011	EDLQDVGVFLHKL	EE loop, α-helix E
5R11	GWFLHKLSQILKK	α-Helix E
5R12	EKEKKDNNIPLQT	C-terminal segment
Antp	RQIKIWFNRRMKWK	Antennapedia homeodomain cell-permeating segment

^aSecondary structure elements of the TIR domain are indicated by consecutive letters, starting from the most N-terminal element.

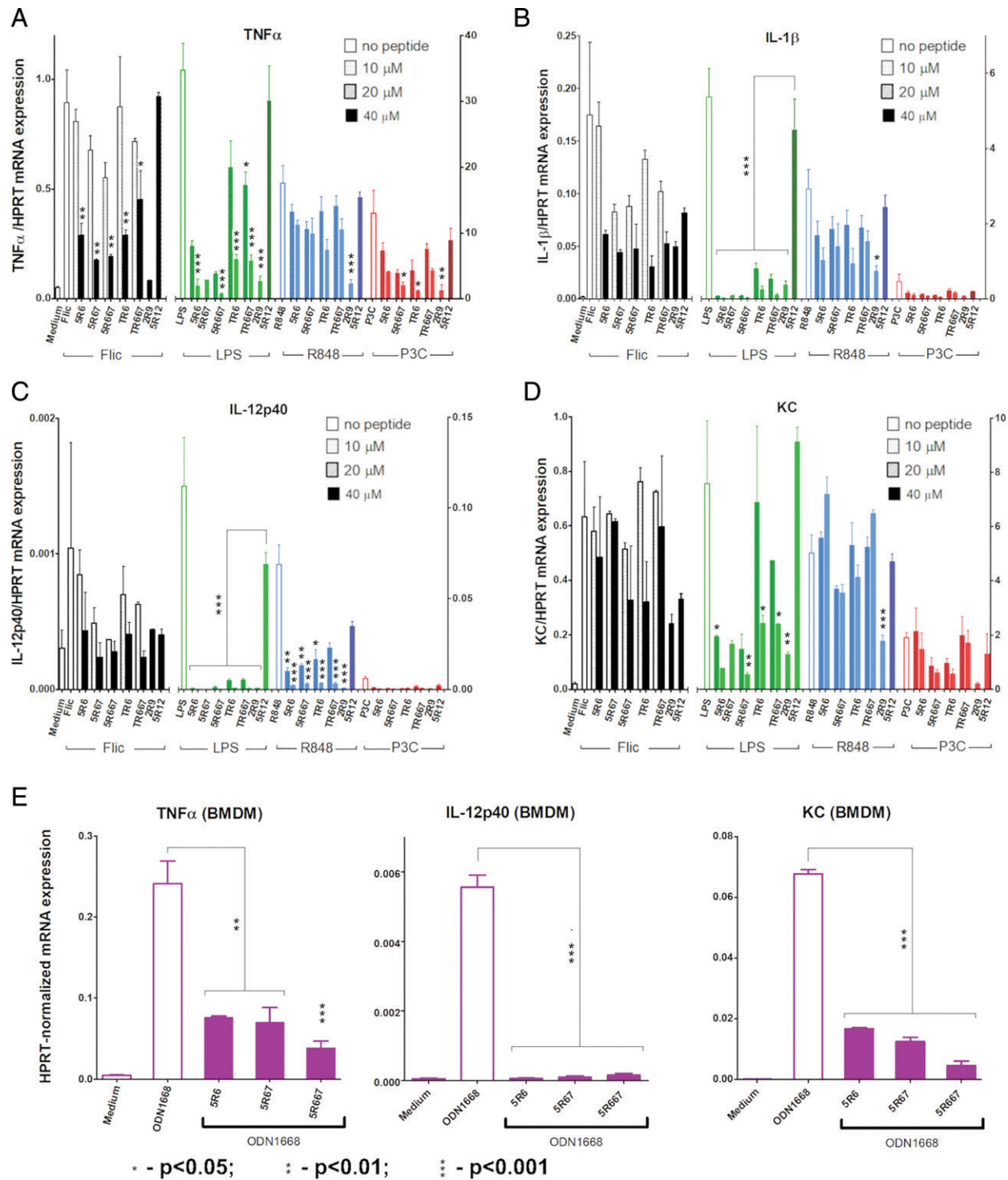


FIGURE 2. Effects of TLR5-derived peptides on cytokine expression elicited by TLR2, TLR4, TLR7, and TLR9 agonists. Primary peritoneal macrophages (A–D) or BMDMs (E) were pretreated with decoy peptides for 30 min and stimulated with FliC, LPS, R848, P3C, or ODN1668 at 1 μ M. mRNA was extracted 1 h after TLR stimulation. Data are presented as mean \pm SE. *p* values are calculated for the difference with control peptide (5R12)-treated cells (A–D) or cells stimulated with ODN1668 but not treated with a peptide (E).

IKK isoforms (Fig. 3C). Notably, the ERK phosphorylation induced by R848 was not affected by 5R667 or TR667 (Fig. 3C). The drastic effect of decoy peptides on IL-6 expression and MAPK activation cannot be explained by a loss of cell viability—the viability assessed by the MTT assay was not affected significantly by peptides at 20 μ M (Fig. 3D). A prolonged incubation in the presence of TR667 at 40 μ M and, to a lesser extent, in the presence of 5R667, however, led to decreased viability (Fig. 3D).

Presented data suggest that 5R6 and its modifications are multi-specific inhibitors of TLRs—in addition to inhibition of TLR5 in peritoneal macrophages and a reporter cell line, these peptides inhibit TLR2, TLR4, and TLR9, but not TLR7. Peptides were selective toward cytokines, because KC expression was not as strongly affected as the expression of TNF- α , IL-1 β , IL-6, or IL-12p40. Effects of inhibitory peptides were less significant in conditions associated with a weaker response to TLR stimulation.

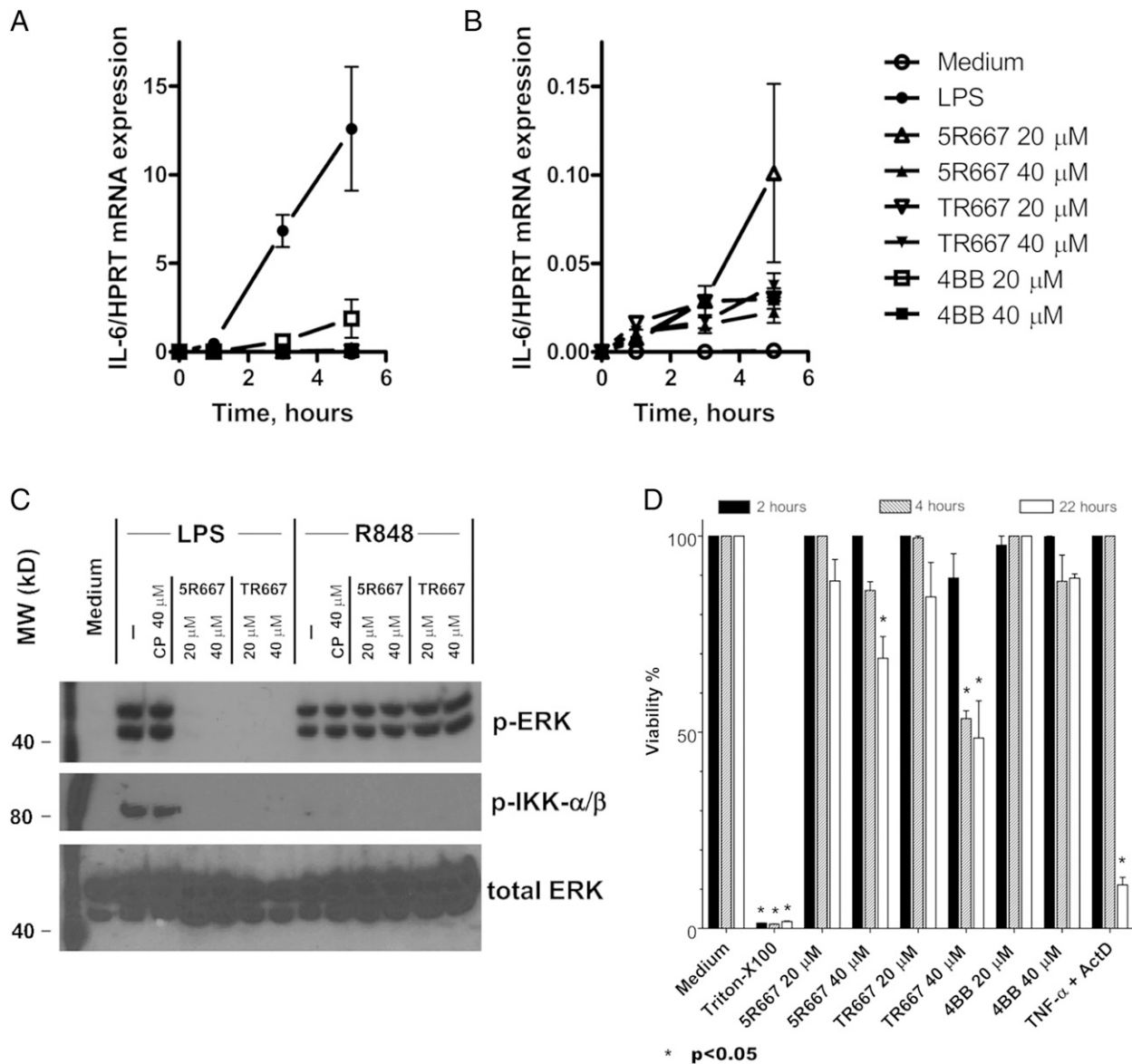


FIGURE 3. Effects of decoy peptides on TLR-induced late cytokine expression, protein phosphorylation, and cell viability. Primary peritoneal macrophages (A–C) were pretreated with decoy peptides for 30 min and stimulated with LPS (100 ng/ml) or R848 (5 μ M). (A, B) mRNA was extracted 1, 3, and 5 h after LPS stimulation. Data from the same experiments are shown in (A) and (B), except that the y-axis of (B) is 1% of that in (A). (C) Cells were lysed 30 min after TLR stimulation. 5R12 served as the control peptide (CP) in these experiments. (D) Viability of primary peritoneal macrophages was measured by MTT assay after incubation of cells in the presence of decoy peptides for 2, 4, or 22 h. (A, B, D) Data are presented as mean \pm SE.

In vivo effects of 5R667 and TR667

Peptides 5R667 and TR667 were further tested for the ability to inhibit systemic cytokine response elicited in mice by administration of TLR agonists. In the first series of experiments, cytokine response was elicited by i.p. administration of FliC to wild-type or NLRC4-deficient mice. Antp peptide, the cell-permeating segment of Antennapedia homeodomain without a TIR-derived decoy sequence (Table I), was used as a control in these series. Peptides were administered at a dose of 200 nmol per animal 1 h prior to FliC administration. Neither of the tested peptides caused a statistically significant change in the circulating cytokine levels in these experiments (Supplemental Fig. 1). It should be noted that the FliC-induced cytokine responses to i.p. FliC administration were quite similar in amplitude and kinetics in the wild-type and NLRC4-deficient animals (Supplemental Fig. 1), suggesting that the cytokine activation is mainly through TLR5 in these experiments.

5R667 and TR667 also were tested for the ability to inhibit the LPS-induced cytokine activation in mice. LPS was used at the high dose of 10 μ g per injection in these experiments. Peptide 4BB, a cell-permeating decoy peptide derived from the BB loop of TLR4 (10, 36), was used as a positive inhibition control in these experiments. LPS elicited a significantly stronger cytokine response than FliC (Supplemental Figs. 1 and 4). Pretreatment of mice with 5R667 or TR667 decreased the LPS-induced TNF- α and IL-12p40 activation; however, the effect of these peptides was less than that induced by 4BB (Fig. 4A, 4B). It should be also noted that the peptides selectively affected expression of individual cytokines—unlike in the cell culture experiments shown in Figs. 3A and 3B, both peptides did not affect the circulating IL-6 statistically significantly (Fig. 4C). We explain this discrepancy by the complexity of IL-6 expression control (35) together with the observed incomplete inhibition of early LPS-induced cytokine expression in vivo (e.g., Fig. 4A).

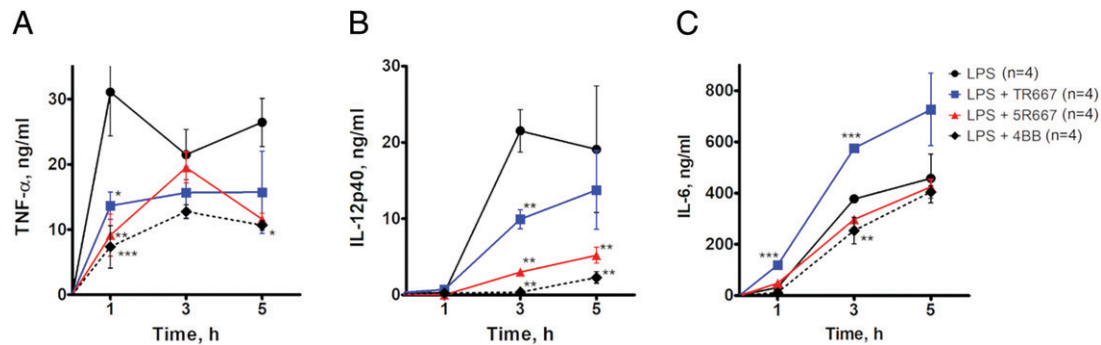


FIGURE 4. Effects of decoy peptides on systemic levels of TNF- α (A), IL-12p40 (B), and IL-6 (C) elicited by LPS administration. C57BL/6J mice were mock treated or treated with the indicated peptides at a dose of 200 nmol. Cytokine secretion was induced by i.p. administration of LPS (10 μ g) 1 h after peptide pretreatment. Data are presented as mean \pm SE. * p < 0.05; ** p < 0.01; *** p < 0.001. p values were calculated for the time-matching differences of LPS-stimulated cytokine levels in the peptide-treated mice with the levels in mice not pretreated with a peptide.

A cell-based Förster resonance energy transfer (FRET) assay of peptide–TIR interactions

TIR domains often demonstrate multispecific binding, being able to interact with similar affinities with a subset of TIRs; a similar binding pattern was observed for TIR interactions with TIR-derived decoy peptides (14). We studied interactions of TIR domains with peptides 5R667 and TR667 using the cell-based FRET/FLIM assay; in this assay, host cells that ectopically express a TIR domain, which is fused with Cer, are treated with a decoy peptide labeled with a spectrally matching Cer fluorescence acceptor (37). In this system, the direct TIR-peptide binding manifests in a decreased Cer fluorescence lifetime due to FRET (10). Peptides were labeled with Cy3 as reported previously (19). Fig. 5A and 5B demonstrate corresponding fluorescence intensity and fluorescence lifetime images of HeLa cells expressing TIR5-Cer and treated with varied doses of 5R667 or TR667. Both

peptides dose dependently decreased the fluorescence lifetime of the TLR5-Cer construct (Fig. 5A, 5B, and Table II), whereas the fluorescence lifetime of Cer not fused to a TIR was not comparably affected by these peptides (Fig. 5D, Table II). Analogous measurements for the Cer-labeled TIRAP and MyD88 TIR domains demonstrated that 5R667 and TR667 also bound TIRAP and MyD88 TIR (Supplemental Fig. 2 and Table II). It could be noted that FRET observed for TLR5-, TIRAP-, or MyD88-Cer constructs in the presence of 5R667 or TR667 was significantly lower than that for TIRAP-Cer in the presence of Cy3-2R9, a previously identified TIR-peptide pair that binds with a high affinity (29) (Table II, Supplemental Fig. 2). The presented findings demonstrate that 5R667 and TR667 bind several TIR domains (namely TLR5, MyD88, and TIRAP TIRs) and agree with the multispecific TLR inhibition profile exhibited by these peptides (Fig. 2).

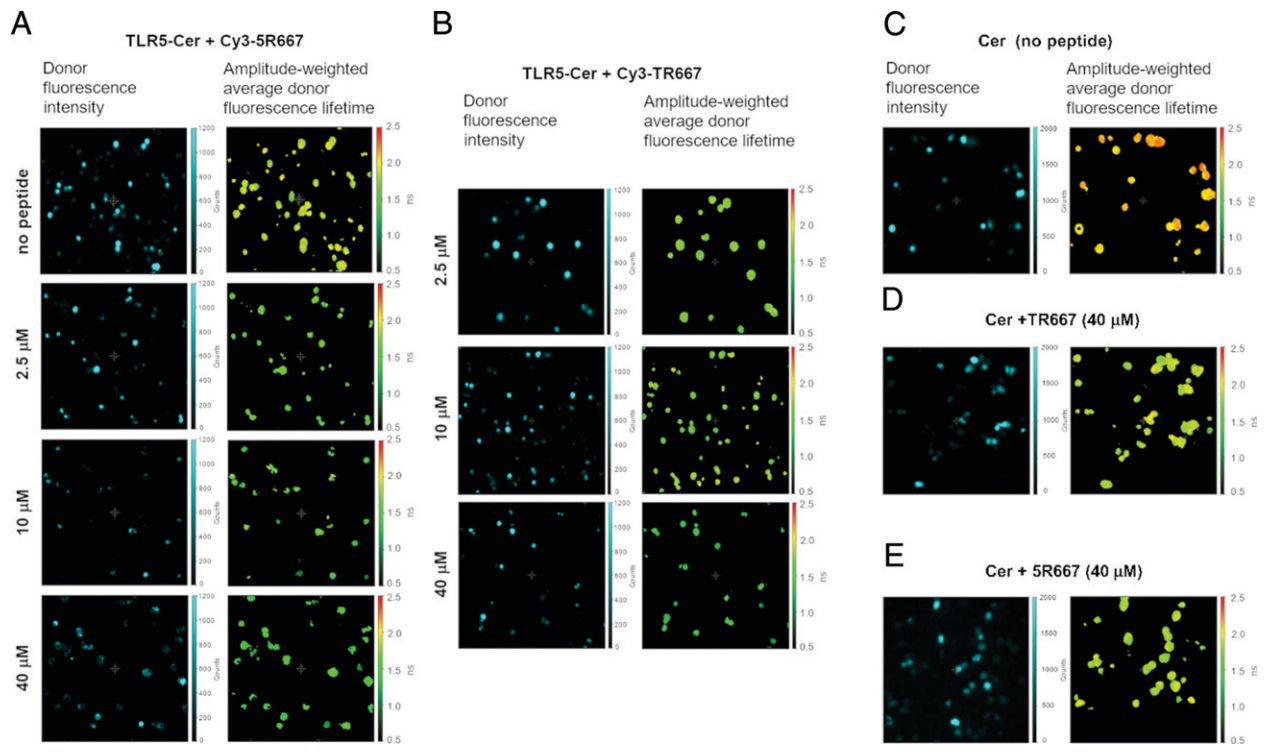


FIGURE 5. Cerulean fluorescence lifetime images of HeLa cells expressing TLR5 TIR-fused Cer (A and B) or Cer not fused to a TIR (C–E) and treated with Cy3-labeled 5R667 or TR667. HeLa cells were transiently transfected with pcDNA3.1 vector encoding either Cer or TIR5-Cer fusion. Two days after transfection, cells were treated with the indicated peptides for 1 h, washed, and fixed. Images were acquired and analyzed using the Alba 5 FLIM system and VistaVision Suite software (ISS, Inc., Champagne, IL). Fluorescence was excited using a 443-nm laser and detected through the 485/35 bandpass filter.

Table II. Effect of Cy3-labeled decoy peptides on amplitude-weighted average fluorescence lifetime of Cer fused or not fused to a TIR domain

Donor	A-WAFL [ns] (without acceptor)	Acceptor	A-WAFL [ns] (in the acceptor presence)		
			Acceptor concentration (μM)		
			2.5	10	40
TLR5-Cer	1.88 ± 0.08	Cy3-5R667	1.86 ± 0.16	1.73 ± 0.11	1.43 ± 0.33
		Cy3-TR667	1.80 ± 0.10	1.76 ± 0.16	1.51 ± 0.31
		Cy3-5R667	1.85 ± 0.27	1.72 ± 0.37	1.27 ± 0.30
TIRAP-Cer	2.03 ± 0.08	Cy3-TR667	1.87 ± 0.27	1.64 ± 0.35	1.38 ± 0.50
		Cy3-2R9	1.83 ± 0.26	1.54 ± 0.26	0.64 ± 0.19
		Cy3-5R667	1.94 ± 0.21	1.72 ± 0.30	1.60 ± 0.35
MyD88-Cer	1.96 ± 0.16	Cy3-5R667	1.89 ± 0.20	1.82 ± 0.24	1.69 ± 0.19
		Cy3-TR667	—	1.92 ± 0.08	1.82 ± 0.14
		Cy3-TR667	—	1.86 ± 0.06	1.92 ± 0.11
Cer	2.07 ± 0.11	Cy3-5R667	—	—	1.82 ± 0.08
		Cy3-TR667	—	—	—
		Cy3-2R9	—	—	—

For each condition, A-WAFL values were calculated based on pixel-by-pixel analysis of 2–3 FLIM images acquired in independent experiments, using VistaVision Suite software (Vista, version 212, ISS). A-WAFL, amplitude-weighted average fluorescence lifetime.

Structural basis for 5R667- and TR667-mediated inhibition

Fig. 6 demonstrates the location and most surface-exposed residues of TLR5 and TIRAP segments that correspond to 5R667 and TR667 peptides. Both peptide-corresponding segments form the second helix (designated as αC'') of the region between β-strands C and D of the cognate TIR domain (Fig. 6A, 6B). Notably, in both cases, the inhibitory segments formed a large patch of the TIR surface (Fig. 6C, 6D). Our previous study has determined that the segments that correspond to both inhibitory peptides are highly conserved among diverse species of Chordates (33) (Supplemental Fig. 3). Thus, the evolutionary conserved consensus sequence for the TLR5 region that corresponds to 5R667 across species that present TLR5 was W₉CL₆EA₉FS₃(Y₃/L₂/F₃)AS₉(S₆/G₁)RS₉ (the frequencies of occurrence of individual residues are indicated in subscript in tenth parts), whereas the corresponding TIRAP motif was

W₉CL₆(K₅/R₂)YS₉QS₈MS₉(H₅/L₄)QS₈AS₉(T₂/S₃/A₃)ES₈ (Supplemental Fig. 3). Note that residues, which are located on the surface-exposed side of αC'' helices (underlined in the previous sentence), are highly conserved (Fig. 6).

Discussion

The initial screening of TLR5-derived, cell-permeable decoy peptides for TLR5 signaling inhibition has identified three peptides that suppress the signaling in a reporter cell line: peptides 5R6, 5R7, and 5R11 (Fig. 1B). Further studies have localized the inhibitory activity of 5R6 and 5R7 to their border region: peptide, which included the C-terminal part of 5R6 and the N-terminal part of the 5R7 decoy, inhibited the signaling more potently than prototypes or 5R11 (Figs. 1C and 2). This peptide, termed “5R667,” inhibited several TLRs. In addition to TLR5, 5R667 suppressed the TLR4- and TLR2-induced activation of TNF-α in primary peritoneal macrophages; however, the peptide did not block the TLR7-mediated TNF-α expression or MAPK activation (Figs. 2A and 3C). The IL12-p40 mRNA was not induced significantly by flagellin or P3C at the early time point (1 h after stimulation), whereas IL12-p40 inhibition in conditions when the gene was robustly induced by LPS or R848 was profound (Figs. 2C and 4B). KC activation by flagellin, R848, or P3C, unlike the LPS-induced KC, was not significantly affected by TLR5 peptides (Fig. 2D). The gene-specific differences in sensitivity can be accounted for by differences in promoter organization; thus, in addition to NF-κB, the KC promoter is regulated by activating protein 1, CAAT/enhancer-binding protein β, C/EBP homologous protein, and CREB and is, in resting macrophages, repressed by NF-κB repressing factor (see Reference 38 for a recent review).

Primary peritoneal macrophages do not robustly respond to TLR9 stimulation (13); therefore, we used BMDMs to evaluate effects of 5R667 on the TLR9 signaling. 5R667 potentially inhibited the ODN1668-induced expression of TNF-α, IL-12p40, and KC mRNA (Fig. 2E), whereas effects of 5R667 on the FliC-induced cytokine expression in BMDMs were insignificant due to weak induction. The presented data suggest that 5R667 inhibits NF-κB-, MyD88-dependent cytokines that are strongly induced at the early time points; however, our observations also indicate the importance of gene-specific expression regulation mechanisms in determining the outcomes of peptide-mediated interference with TLR signaling.

Our previous survey of TIR domain sequences (33) has identified an evolutionarily conserved TIRAP motif that corresponds to one of four interfaces that are important for the TIRAP-mediated signaling and self-assembly of TIRAP oligomers in solution (12). Structurally, this TIRAP motif exactly corresponded to the TLR5 sequence segment represented by 5R667 (Fig. 6A, 6B). A peptide derived from

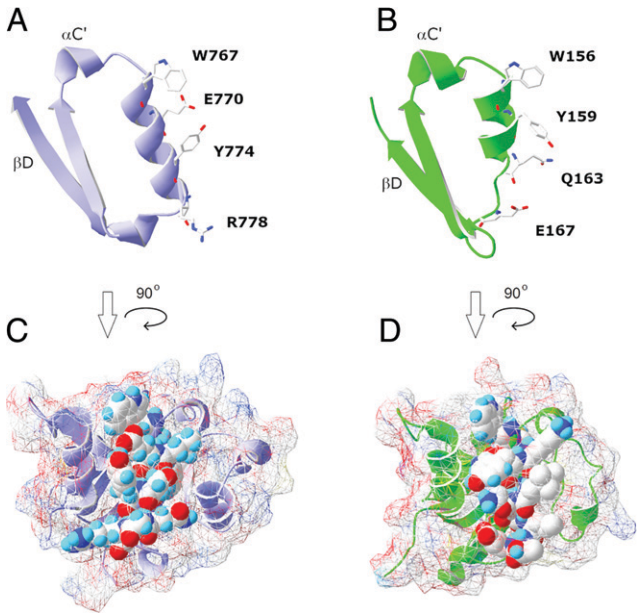


FIGURE 6. Peptides 5R667 and TR667 derive from αC'' helices of corresponding TIR domains. (A and B) TLR5 (A) and TIRAP (B) TIR segments that correspond to decoy peptides 5R667 and TR667 form the second helix of the region between β-strands C and D. Backbone segments that include β-strands C and D and the helical region between them are shown in ribbon style. Side chains are shown only for the evolutionarily conserved surface-exposed residues. (C and D) TLR5 (C) and TIRAP (D) TIR models with segments that correspond to 5R667 and TR667 are shown in the space-filling mode in CPK (Corey-Pauling-Koltun) colors.

this TIRAP region, TR667, inhibited induction of TNF- α elicited by LPS; yet, its effects on KC induction were less. Generally, 5R667 and TR667 demonstrated similar properties: both peptides inhibited multiple TLRs, and the inhibition was more pronounced with respect to proinflammatory cytokines that are strongly induced by TLR stimulation (TNF- α , IL-1 β , and IL-12p40). These observations were further supported by our in vivo experiments. 5R667 and TR667 did not significantly affect the FliC-induced cytokine expression in live mice (Supplemental Fig. 1). The absence of a significant effect can be accounted for by a relatively weak inhibition of the FliC-induced signaling in peritoneal macrophages (Fig. 2A–2D). Of note is that FliC induced similar cytokine levels in wild-type and NLRC4-deficient mice (Supplemental Fig. 1), indicating that the TLR-mediated cytokine activation was predominant in this model. LPS elicited 5–100 times higher levels of circulating cytokines than FliC (Fig. 4 and Supplemental Fig. 1). The sharp induction of TNF- α and IL-12p40 by LPS was significantly inhibited by 5R667 and TR667; however, the inhibition was less than that by 4BB, a TLR4-derived peptide previously shown to potently inhibit TLR4 signaling (10, 36).

The observed multispecific TLR inhibition by peptides 5R667 and TR667 is in concert with the results of peptide-TIR binding studies: both inhibitory peptides quenched fluorescence of all TIR-Cer constructs tested, but not the fluorescence of Cer not fused to a TIR, with 5R667 demonstrating a slightly better quenching (Table II). The ability of 5R667 and TR667 to bind TIRs of common TLR adapters (Table II and Supplemental Fig. 2) accounts for the multispecific TLR inhibition pattern exhibited by these peptides.

Our previous study—which computationally analyzed 26,414 publicly available TIR domain sequences and hierarchically classified them into groups and subgroups, based on algorithmically determined sequence motifs that best distinguish each group—clustered TLR5 and TIRAP TIR domains into separate groups (33). The results of that computational study demonstrated that the TIR region represented by 5R667 (similarly to the TIRAP TR667 region) is highly conserved among TLR5 orthologs (Supplemental Fig. 3 and Reference 33), with surface-exposed residues of TLR5 and TIRAP C' helices forming following highly conserved motifs: -W-x (2)-E-x (3)-(Y3/L2/F3)-x(3)-R- and -W-x (2)-Y-x (3)-Q-x (3)-E-, respectively. Moreover, these evolutionarily conserved motifs are distinctive for TLR5 and TIRAP orthologs (Supplemental Fig. 3 and Fig. 6A, 6B). The results of our peptide screenings confirm the four-residue motif identified by analysis of evolutionary sequence variability. Thus, peptide 5R67, which includes three of the four conserved surface-exposed residues, was less active than 5R667; furthermore, 5R6 and 5R7 (each containing two of the motif residues) were even less active (Figs. 1 and 2).

Locations of conserved motifs, which correspond to inhibitory peptides, overlap with one of four TIR interfaces previously proposed to mediate the assembly of TLR signaling complexes. The TIR interaction site, which includes the R667 peptides, encompasses C and B helices and was previously defined as “site 2” (13, 14) or “BC surface” (12). This site was proposed to interact with site 3 located within or near D helices of the interaction counterpart (12–14, 39). In conclusion, this study identifies a new inhibitory decoy peptide, which corresponds to an evolutionarily conserved adapter binding site of TLR5 TIR domains. This peptide inhibits signaling by multiple TLRs by binding to and sequestering TLR adapters TIRAP and MyD88.

Acknowledgments

We thank Dr. Stefanie N. Vogel for providing highly purified LPS, Dr. Wenji Piao for engineering the expression vector encoding TLR5 TIR fused with Cerulean fluorescent protein, and Dr. Megan A. Rizzo for originally providing Cerulean expression vector.

Disclosures

The authors have no financial conflicts of interest.

References

- Kawai, T., and S. Akira. 2011. Toll-like receptors and their crosstalk with other innate receptors in infection and immunity. *Immunity* 34: 637–650.
- Janeway, C. A., Jr., and R. Medzhitov. 2002. Innate immune recognition. *Annu. Rev. Immunol.* 20: 197–216.
- Gewirtz, A. T., T. A. Navas, S. Lyons, P. J. Godowski, and J. L. Madara. 2001. Cutting edge: bacterial flagellin activates basolaterally expressed TLR5 to induce epithelial proinflammatory gene expression. *J. Immunol.* 167: 1882–1885.
- Hayashi, F., K. D. Smith, A. Ozinsky, T. R. Hawn, E. C. Yi, D. R. Goodlett, J. K. Eng, S. Akira, D. M. Underhill, and A. Aderem. 2001. The innate immune response to bacterial flagellin is mediated by Toll-like receptor 5. *Nature* 410: 1099–1103.
- Franchi, L., A. Amer, M. Body-Malapel, T. D. Kanneganti, N. Özören, R. Jagirdar, N. Inohara, P. Vandenabeele, J. Bertin, A. Coyle, et al. 2006. Cytosolic flagellin requires Ipaf for activation of caspase-1 and interleukin 1 β in *Salmonella*-infected macrophages. *Nat. Immunol.* 7: 576–582.
- Miao, E. A., C. M. Alpujch-Aranda, M. Dors, A. E. Clark, M. W. Bader, S. I. Miller, and A. Aderem. 2006. Cytoplasmic flagellin activates caspase-1 and secretion of interleukin 1 β via Ipaf. *Nat. Immunol.* 7: 569–575.
- Andrade, W. A., and D. S. Zamboni. 2020. NLRC4 biology in immunity and inflammation. *J. Leukoc. Biol.* 108: 1117–1127.
- Choi, Y. J., E. Im, H. K. Chung, C. Pothoulakis, and S. H. Rhee. 2010. TRIF mediates Toll-like receptor 5-induced signaling in intestinal epithelial cells. *J. Biol. Chem.* 285: 37570–37578.
- Jin, M. S., and J. O. Lee. 2008. Structures of the Toll-like receptor family and its ligand complexes. *Immunity* 29: 182–191.
- Toshchakov, V. Y., H. Szmazinski, L. A. Couture, J. R. Lakowicz, and S. N. Vogel. 2011. Targeting TLR4 signaling by TLR4 Toll/IL-1 receptor domain-derived decoy peptides: identification of the TLR4 Toll/IL-1 receptor domain dimerization interface. *J. Immunol.* 186: 4819–4827.
- Gay, N. J., M. F. Symmons, M. Gangloff, and C. E. Bryant. 2014. Assembly and localization of Toll-like receptor signalling complexes. *Nat. Rev. Immunol.* 14: 546–558.
- Ve, T., P. R. Vajihala, A. Hedger, T. Croll, F. DiMaio, S. Horsefield, X. Yu, P. Lavrencic, Z. Hassan, G. P. Morgan, et al. 2017. Structural basis of TIR-domain-assembly formation in MAL- and MyD88-dependent TLR4 signaling. *Nat. Struct. Mol. Biol.* 24: 743–751.
- Javmen, A., H. Szmazinski, J. R. Lakowicz, and V. Y. Toshchakov. 2018. Blocking TIR domain interactions in TLR9 signaling. *J. Immunol.* 201: 995–1006.
- Toshchakov, V. Y., and A. Javmen. 2020. Targeting the TLR signalosome with TIR domain-derived cell-permeable decoy peptides: the current state and perspectives. *Innate Immun.* 26: 35–47.
- Murphy, G., and D. A. Isenberg. 2019. New therapies for systemic lupus erythematosus - past imperfect, future tense. [Published erratum appears in 2019 *Nat. Rev. Rheumatol.* 15: 509.] *Nat. Rev. Rheumatol.* 15: 403–412.
- Mahjoubin-Tehran, M., S. Rezaei, A. Jalili, S. H. Aghae-Bakhtiari, H. M. Orafi, T. Jamialahmadi, and A. Sahebkar. 2020. Peptide decoys: a new technology offering therapeutic opportunities for breast cancer. *Drug Discov. Today* 25: 593–598.
- Toshchakov, V. Y., and S. N. Vogel. 2007. Cell-penetrating TIR BB loop decoy peptides a novel class of TLR signaling inhibitors and a tool to study topology of TIR-TIR interactions. *Expert Opin. Biol. Ther.* 7: 1035–1050.
- Copolovici, D. M., K. Langel, E. Eriste, and Ü. Langel. 2014. Cell-penetrating peptides: design, synthesis, and applications. *ACS Nano* 8: 1972–1994.
- Javmen, A., H. Szmazinski, J. R. Lakowicz, and V. Y. Toshchakov. 2020. Frontline science: targeting the TLR7 signalosome assembly. *J. Leukoc. Biol.* 108: 1697–1706.
- Gewirtz, A. T., P. O. Simon, Jr., C. K. Schmitt, L. J. Taylor, C. H. Hagedorn, A. D. O'Brien, A. S. Neish, and J. L. Madara. 2001. *Salmonella typhimurium* translocates flagellin across intestinal epithelia, inducing a proinflammatory response. *J. Clin. Invest.* 107: 99–109.
- McSorley, S. J., B. D. Ehst, Y. Yu, and A. T. Gewirtz. 2002. Bacterial flagellin is an effective adjuvant for CD4⁺ T cells in vivo. *J. Immunol.* 169: 3914–3919.
- Sanders, C. J., L. Franchi, F. Yarovsky, S. Uematsu, S. Akira, G. Núñez, and A. T. Gewirtz. 2009. Induction of adaptive immunity by flagellin does not require robust activation of innate immunity. *Eur. J. Immunol.* 39: 359–371.
- Derossi, D., A. H. Joliet, G. Chassaing, and A. Prochiantz. 1994. The third helix of the Antennapedia homeodomain translocates through biological membranes. *J. Biol. Chem.* 269: 10444–10450.
- Pace, C. N., F. Vajdos, L. Fee, G. Grimsley, and T. Gray. 1995. How to measure and predict the molar absorption coefficient of a protein. *Protein Sci.* 4: 2411–2423.
- Couture, L. A., W. Piao, L. W. Ru, S. N. Vogel, and V. Y. Toshchakov. 2012. Targeting Toll-like receptor (TLR) signaling by Toll/interleukin-1 receptor (TIR) domain-containing adapter protein/MyD88 adapter-like (TIRAP/Mal)-derived decoy peptides. *J. Biol. Chem.* 287: 24641–24648.
- Toshchakov, V. U., S. Basu, M. J. Fenton, and S. N. Vogel. 2005. Differential involvement of BB loops of toll-IL-1 resistance (TIR) domain-containing adapter proteins in TLR4- versus TLR2-mediated signal transduction. *J. Immunol.* 175: 494–500.
- Szmazinski, H., V. Toshchakov, W. Piao, and J. R. Lakowicz. 2013. Imaging of protein secretion from a single cell using plasmonic substrates. *Bionanoscience* 3: 30–36.
- Piao, W., S. N. Vogel, and V. Y. Toshchakov. 2013. Inhibition of TLR4 signaling by TRAM-derived decoy peptides in vitro and in vivo. *J. Immunol.* 190: 2263–2272.

29. Piao, W., K. A. Shirey, L. W. Ru, W. Lai, H. Szmazinski, G. A. Snyder, E. J. Sundberg, J. R. Lakowicz, S. N. Vogel, and V. Y. Toshchakov. 2015. A decoy peptide that disrupts TIRAP recruitment to TLRs is protective in a murine model of influenza. *Cell Rep.* 11: 1941–1952.
30. Baek, M., F. DiMaio, I. Anishchenko, J. Dauparas, S. Ovchinnikov, G. R. Lee, J. Wang, Q. Cong, L. N. Kinch, R. Dustin Schaeffer, et al. 2021. Accurate prediction of protein structures and interactions using a three-track neural network. *Science* 373: 871–876.
31. Berman, H. M., T. Battistuz, T. N. Bhat, W. F. Bluhm, P. E. Bourne, K. Burkhardt, Z. Feng, G. L. Gilliland, L. Iype, S. Jain, et al. 2002. The Protein Data Bank. *Acta Crystallogr. D Biol. Crystallogr.* 58: 899–907.
32. Guex, N., and M. C. Peitsch. 1997. SWISS-MODEL and the Swiss-PdbViewer: an environment for comparative protein modeling. *Electrophoresis* 18: 2714–2723.
33. Toshchakov, V. Y., and A. F. Neuwald. 2020. A survey of TIR domain sequence and structure divergence. [Published erratum appears in 2022 *Immunogenetics* 74: 269.] *Immunogenetics* 72: 181–203.
34. Hirschfeld, M., J. J. Weis, V. Toshchakov, C. A. Salkowski, M. J. Cody, D. C. Ward, N. Qureshi, S. M. Michalek, and S. N. Vogel. 2001. Signaling by Toll-like receptor 2 and 4 agonists results in differential gene expression in murine macrophages. *Infect. Immun.* 69: 1477–1482.
35. Faggioli, L., C. Costanzo, M. Donadelli, and M. Palmieri. 2004. Activation of the interleukin-6 promoter by a dominant negative mutant of c-Jun. *Biochim. Biophys. Acta* 1692: 17–24.
36. Toshchakov, V. Y., M. J. Fenton, and S. N. Vogel. 2007. Cutting edge: differential inhibition of TLR signaling pathways by cell-permeable peptides representing BB loops of TLRs. *J. Immunol.* 178: 2655–2660.
37. Szmazinski, H., V. Toshchakov, and J. R. Lakowicz. 2014. Application of phasor plot and autofluorescence correction for study of heterogeneous cell population. *J. Biomed. Opt.* 19: 046017.
38. Jundi, K., and C. M. Greene. 2015. Transcription of interleukin-8: How altered regulation can affect cystic fibrosis lung disease. *Biomolecules* 5: 1386–1398.
39. Clabbers, M. T. B., S. Holmes, T. W. Muusse, P. R. Vajjhala, S. J. Thygesen, A. K. Malde, D. J. B. Hunter, T. I. Croll, L. Flueckiger, J. D. Nanson, et al. 2021. MyD88 TIR domain higher-order assembly interactions revealed by microcrystal electron diffraction and serial femtosecond crystallography. *Nat. Commun.* 12: 2578.